Journal Pre-proof

The removal of arsenic from solution through biochar-enhanced precipitation of calcium-arsenic derivatives

Eric F. Zama, Gang Li, Yu-Ting Tang, Brian J. Reid, Ngwa M. Ngwabie, Gou-Xin Sun

Please cite this article as: Zama, E.F., Li, G., Tang, Y.-T., Reid, B.J., Ngwabie, N.M., Sun, G.-X., The removal of arsenic from solution through biochar-enhanced precipitation of calcium-arsenic derivatives, *Environmental Pollution* (2021), doi: https://doi.org/10.1016/j.envpol.2021.118241.

This is a PDF file of an article that has undergone enhancements after acceptance, such as the addition of a cover page and metadata, and formatting for readability, but it is not yet the definitive version of record. This version will undergo additional copyediting, typesetting and review before it is published in its final form, but we are providing this version to give early visibility of the article. Please note that, during the production process, errors may be discovered which could affect the content, and all legal disclaimers that apply to the journal pertain.

Author Statement

Eric Fru Zama and **Gou-Xin Sun** conceived and planned the research and experiments. **Eric Fru Zama** took the lead in carrying out the experiments and writing the manuscript. **Gang Li** and **Brian J. Reid**, supervised the research and carried out review of the manuscript drafts. **Yu-Ting Tang** contributed to samples preparation and laboratory analysis. **Martin Ngwabie** verified and validated the analytical methods and helped in processing the experimental data. All authors were involved in discussing the results of the study and commented on the manuscript.

Graphical Abstract
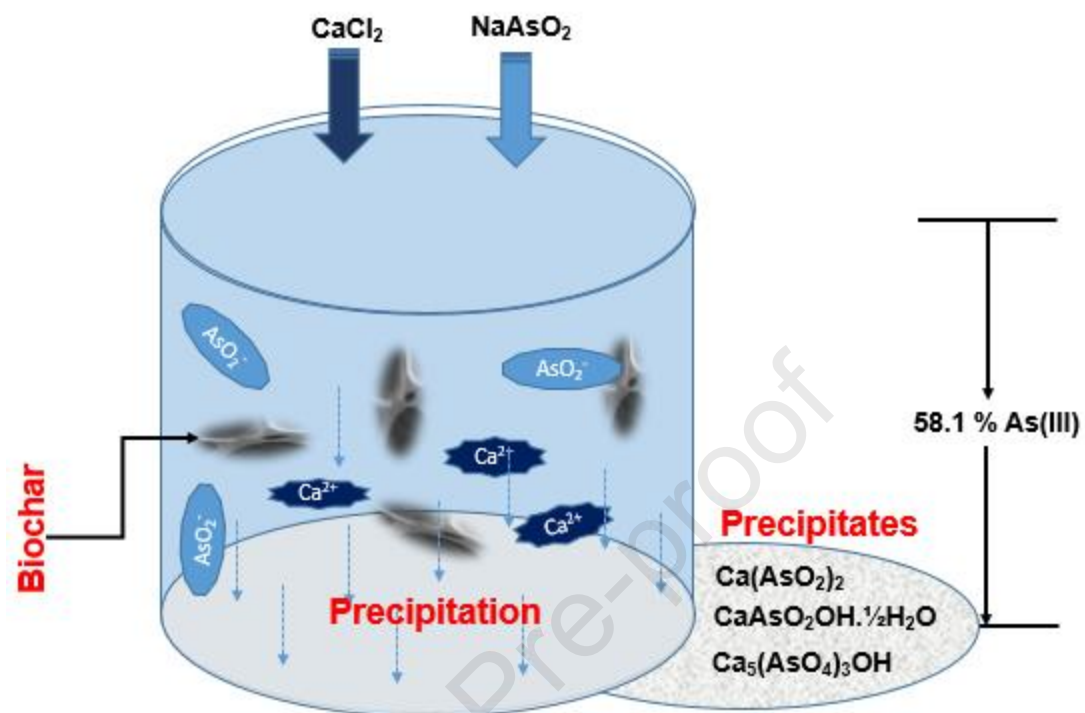
The removal of arsenic from solution through biochar-enhanced precipitation of calcium-arsenic derivatives

Eric F. Zama[2, 3], Gang Li[3], Yu-Ting Tang[4], Brian J. Reid[5], Ngwa M. Ngwabie[2], Gou-Xin Sun[1*]

[1] State Key Lab of Urban and Regional Ecology, Research Center for Eco-Environmental Sciences, Chinese Academy of Sciences, Beijing 100085, P.R. China

[2] College of Technology, Department of Agricultural and Environmental Engineering, University of Bamenda, P.O. Box 39 Bambili.

[3] Zhejiang Key Lab of Urban Environmental Processes and Pollution control, Ningbo Urban Environmental Observatory and Research Station, Chinese Academy of Science, Ningbo 361021, China

[4] School of Geographical Science, Faculty of Science and Engineering, University of Nottingham, Ningbo China, 315100, Ningbo, China

[5] School of Environmental Sciences, University of East Anglia, Norwich Research Park, Norwich NR4 7TJ, UK

*Corresponding author

Guo-Xin Sun: email; gxsun@rcees.ac.cn , Tel: +86 62849328

23 **Abstract**

24 Arsenic (As) pollution remains a major threat to the quality of global soils and drinking

25 water. The health effects of As pollution are often severe and have been largely reported

26 across Asia and South America. This study investigated the possibility of using unmodified

27 biochar derived from rice husk (RB) and aspen wood (WB) at 400 °C and 700 °C to enhance

28 the precipitation of calcium/arsenic compounds for the removal of As(III) from solution. The

29 approach was based on utilizing calcium to precipitate arsenic in solution and adding

30 unmodified biochar to enhance the process. Using this approach, As(III) concentration in

31 aqueous solution decreased by 58.1 % when biochar was added, compared to 25.4 % in the

32 absence of biochar. Varying the pH from acidic to alkaline enabled an investigation into the

33 pH dependent dynamics of the approach. Results indicated that significant precipitation was

34 only possible at near neutral pH (i.e. pH = 6.5) where calcium arsenites (i.e. $Ca(AsO_2)_2$, and

35 $CaAsO_2OH \cdot \frac{1}{2}H_2O$) and arsenates (i.e. $Ca_5(AsO_4)_3OH$) were precipitated and deposited as

36 aggregates in the pores of biochars. Arsenite was only slightly precipitated under acidic

37 conditions (pH = 4.5) while no arsenite was precipitated under alkaline conditions (pH =

38 9.5). Arsenite desorption from wood biochar was lowest at pH 6.5 indicating that wood

39 biochar was able to retain a large quantity of the precipitates formed at pH 6.5 compared to

40 pH 4.5 and pH 9.5. Given that the removal of As(III) from solution is often challenging and

41 that biochar modification invites additional cost, the study demonstrated that low cost

42 unmodified biochar can be effective in enhancing the removal of As(III) from the

43 environment through Ca-As precipitation.

44

45 **Key words**

46 Biochar, Arsenic pollution, Precipitation, Calcium arsenite/arsenate, pH

47

1. Introduction

Arsenic (As) pollution is a major threat to the quality of global soils and drinking water. Significantly high amounts of As have been reported in the ground waters of Chile, Mexico, USA, India, Bangladesh and China (Shankar and Shanker, 2014). For example, Huq et al. (2018) recently reported concentrations of arsenic as high as 452 µg L^{-1} in the Datong river basin of China and 590.7 µg L^{-1} in the Kushtia District of Bangladesh. These high levels of As contamination have caused major health risks in humans including cancer, neurological effects and cardiac disorders (Hong et al., 2014).

Arsenic is highly toxic and emitted in the environment (soil, water and air) from anthropogenic activities (e.g. industrial activities, smelting) and natural sources (e.g. weathering of arsenic containing minerals). It exists in the environment mainly in two forms of inorganic oxy-anions (i.e. As(III) (arsenite) and As(V) (arsenate)) (Yokoyama et al., 2012). As(III) is more toxic and prevalent in underground waters than As(V) (Tchounwou et al., 2012; Zama et al., 2018) which is easily removed by conventional methods.

Several technologies have been developed to remove As from the environment especially from drinking water. Mudhoo et al. (2011) described over five conventional methods of As removal including; coagulation with iron salts and alum, lime softening, ion exchange, activated alumina and membrane filtration. The authors highlighted that, adsorption; using carbonaceous materials such as biochar appear to have some advantages over other technologies because of the simple design and sludge-free nature of the technology using the carbonaceous materials. The use of biochar is arguably more cost effective involving low investment in terms of both initial cost and land requirements (Kurniawan et al., 2006). However, the use of biochar without modification for the removal of As from solution has often been ineffective, with reports of slightly increased concentration of As in solution following the addition of biochar (Beesley et al., 2013; Deng et al., 2020; Zheng et al., 2015).

3

73 Biochar modification using agents like Fe (He et al., 2018), Mn (Lin et al., 2017), red mud

74 (Wu et al., 2017) and Ca (Agrafioti et al., 2014), has therefore been tipped as "more

75 effective" in the removal of As from solution. The majority of these modified biochars have

76 removed significant amounts of As from solution. For example, Hu et al. (2015) impregnated

77 hickory biochar with Fe and reported an improvement of sorption capacity from 'no

78 sorption' in the pristine biochar to 2.16 mg g^{-1} in the modified biochar. Recently, He et al.

79 (2018) reported large quantities of iron oxide particles tightly embedded in the porous matrix

80 of corn straw biochar through iron-impregnation. This composition was shown to possess a

81 larger surface area, more functional groups, and greater thermal stability, which exhibited

82 excellent ability of adsorbing As (V) (6.80 mg g^{-1}) compared to the unmodified biochar

83 (0.017 mg g^{-1}).

84 The use of calcite and other calcium-containing compounds to immobilize As in soil or water

85 has been widely reported (Renard et al., 2015; Guan et al., 2009; Yokoyama et al., 2012) and

86 precipitation of arsenites/arsenates or co-precipitation with calcium carbonate (CaCO$_3$) has

87 been considered as the major mechanism involved in this immobilization process (Martínez-

88 Villegas et al.,2013; Renard et al., 2015). It is believed that once As is incorporated into

89 calcite which is not sensitive to redox changes, the As is completely "locked away"

90 compared to iron-arsenic composites which may be affected by redox changes allowing

91 sorbed As to be released back into the environment (Yokoyama et al., 2009).

92 Systemically developing ways to improve the efficiency and the extent of arsenites/arsenates

93 precipitation using calcium-containing compounds remains open for research. The

94 objectives of this study were: (1) to investigate the influence of biochar on the precipitation

95 process of calcium and arsenite as a mechanism for arsenite remediation. (2) To assess the

96 influence of pH conditions (acidic, neutral and alkaline) on the removal process in the

97 presence and absence of biochar. The study was conducted based on the hypothesis that

98 "biochar improves the precipitation process of calcium and arsenite as a mechanism for

99 arsenite remediation and this process is pH dependent".

2. Materials and methods

2.1. Reagents, quality assurance and data analysis

102 All reagents ($CaCl_2$, $NaAsO_2$, NaOH and HNO_3) used in this study were analytical grade.

103 Working solutions were obtained by dissolving designated quantities of reagents in ultra-

104 pure water (Milli-Q, 18.2 MΩ cm, TOC 3 ppb). Treatments were mostly made in triplicates.

105 Solutions without biochar were made as controls. All experiments were carried out at room

106 temperature and pH controlled to the target levels (4.5, 6.5 and 9.5) using 0.1 M HNO_3 or

107 0.1 M NaOH. For data analysis, OriginPro 8.5 (OriginLab, USA), was mainly used while

108 sorption and desorption analysis were calculated using Microsoft excel.

2.2. Biochar preparation

110 Rice husk and aspen wood biomass materials were used to produce biochars at 400 °C and

111 700 °C by slow-dry pyrolysis. The two biomass materials and production temperatures were

112 selected to assess the effects of different properties of biochars on arsenic precipitation. The

113 two wood-based biomass materials (rice husk and wood) were chopped into pieces (< 1 cm)

114 and placed in crucibles mounted in a Neytech Muffle Furnace (Vulcan 3-1750A) with very

115 limited oxygen supply (Wang et al., 2016). The temperature was ramped at 10 °C min^{-1} to

116 the designated pyrolysis temperature and maintained for 4 hours. The resulting biochars were

117 allowed to cool to room temperature and then pulverized to particle sizes between 0.17 and

118 0.45 mm. The biochars were coded RB4, RB7, WB4 and WB7 representing rice husk and

119 aspen wood biochars at 400 °C and 700 °C.

120

121

5

122   **2.3. Sorption experiments**

123   A solution containing 0.02 g L^{-1} NaAsO$_2$ and 1.1 g L^{-1} CaCl$_2$ was prepared by dissolving

124   specific quantities of the reagent in ultra-pure water. The prepared solution was sub-divided

125   into three parts and the pH levels were adjusted to 4.5, 6.5 and 9.5 respectively in order to

126   evaluate the influence of pH on the sorption process. Using 50 mL test tubes, 0.05 g of

127   biochars (RB4, RB7, WB4 and WB7) were added to 20mL of each solution and the

128   treatments were mounted on an end-to-end shaker (150 rpm, 25 °C) for 72 h until

129   equilibrium. The pH of the treatments was regularly adjusted (every 8 h) to the desired levels

130   (i.e. 4.5, 6.5 and 9.5) using 0.1 M NaOH or 0.1 M HNO$_3$. Treatments without biochar were

131   used as controls. After 72 h, the treatments were removed and allowed to settle for 48 h.

132   Syringes and 0.45 μm syringe filters were used to filter the supernatants, which were

133   analysed for As concentration using the Inductively Coupled Plasma Optical Emission

134   Spectrometry (ICP-OES, Optima 2000, PerkinElmer Co., USA). The As-loaded biochars

135   were subsequently dried at 70 °C in an oven for XRD, XPS and FTIR analysis. These post-

136   adsorption biochars were coded RB4c, RB7c, WB4c and WB7c, representing As-loaded rice

137   husk and aspen wood biochars at 400 °C and 700 °C.

138   Two sorption isotherm models (i.e. the Langmuir and the Freundlich sorption models) were

139   tested to explain the sorption behavior of As(III) on all four biochars. Parameters for the

140   isotherms were obtained in batch sorption experiments using varying initial concentrations

141   of As(III) (10 μg L^{-1} to 50 μg L^{-1}). Details of the methods, including the equations used are

142   presented in *supporting materials*.

143   **2.4.Desorption experiments**

144   Desorption experiments were conducted to determine the stability of sorbed arsenic on the

145   biochars over the three pH levels (i.e. pH 4.5, 6.5, and 9.5). Treatments containing 0.05 g

146 (dry mass) of As-loaded biochars in 10 mL of solution were mounted on an end-to-end

147 shaker for 24 h. Syringes and 0.45 μm syringe filters were used obtain supernatants, and

148 desorbed arsenic was measured using ICP-MS (7500a, Agilent Technologies, USA). The

149 quantity of arsenic desorbed from the biochar into solution was used as a measure for the

150 stability of arsenic on the biochar.

151 **2.5. Thermodynamic analysis**

152 Key thermodynamic parameters including Gibbs free energy change ($\Delta \mathbf{G^o}$), enthalpy ($\Delta \mathbf{H^o}$),

153 and entropy change ($\Delta \mathbf{S^o}$) for As(III) sorption on biochars were calculated from equations

154 (1) and (2) (Zama et al., 2017). Temperatures were ranged from 25 °C to 45 °C (298 - 318

155 K). A linear plot of ΔG^o versus T in equation (2) gives values of ΔH^o and ΔS^o from the

156 intercept and slopes respectively (Zama et al., 2017)

$$\Delta \mathbf{G^o} \quad = \quad -RT \, \mathrm{Ln} \mathrm{K_C} \qquad \qquad \textbf{(1)}$$

$$\Delta \mathbf{G^o} \quad = \quad \Delta \mathbf{H^o} - \mathrm{T} \Delta \mathbf{S^o} \qquad \qquad \textbf{(2)}$$

Where: R = the universal gas constant (8.314 J/mol/K), K_C = thermodynamic constant, T = temperature (K).

K_C is dimensionless and obtained by multiplying the Langmuir equilibrium constant (K_L) by 55.5 (moles of

water per liter of solution).

157

158 **2.6. Analysis of physicochemical properties of biochars**

159 *Yield and Ash:* Biochar was heated under oxygen supply at 700 °C for 2 h, in the Neytech

160 Muffle Furnace (Vulcan 3-1750A) for ash content analysis. Yields and ash content were

161 obtained using equations 3 and 4, respectively.

162

$$\% \text{ Yield} = \frac{\mathrm{M_{BC}}}{\mathrm{M_{BM}}} \times 100 \qquad \qquad (3)$$

163

$$\% \text{ Ash} = \frac{\mathrm{M_{ASH}}}{\mathrm{M_{BC}}} \times 100 \qquad \qquad (4)$$

164

Where M_{BC} = mass of biochar, M_{BM} = mass of biomass, M_{ASH} = mass of ash

7

165

166 *Elemental analysis:* Total C, H, S, and N in biochars was measured by dry combustion using

167 Elementar (Vario EL III) while total O was calculated on a difference basis (Yousaf et al.,

168 2017).

169 Changes in carbonization, aromaticity and polarity of biochars were determined from their

170 atomic ratios (i.e. H:C, O:C, (O+N):C and C:N) according to equation 5.

171 $$\text{Atomic ratio} = \frac{Ca/Ma}{Cb/Mb} \qquad (5)$$

172 *Where Ca and Cb are the concentrations of element 'a' and element 'b' respectively as*

173 *obtained from elemental analysis on biochar, Ma and Mb are the molar masses of element*

174 *'a' and element 'b' respectively.*

175 *Surface area, pH, and morphology:* The pH of biochars was obtained by mixing 1 g of

176 biochar in 20 mL of deionized water on an end-to-end shaker at 120 rpm for 4 h and the pH

177 value in the liquid phase was measured using a pH meter (Mettler Toledo 320-S). The

178 morphological and textural properties of biochars were studied using the Field Emission

179 Scanning Electron Microscope equipped with Energy Dispersive X-Ray Spectroscopy (FE

180 SEM-EDX, SU8000). The surface area and porosity of the biochars were measured with the

181 Surface Area and Porosity Analyzer (SAPA, 2020 HD88) by N_2 gas adsorption at 77 K. The

182 total internal surface area of the biochars was then determined by the Brunauer, Emmett

183 and Teller (BET) method (BET surface area) while pore size distribution was

184 characterized by applying the density functional theory (DFT) method to the adsorption

185 isotherm. The volume of N_2 gas adsorbed at a relative pressure (P/P_0 ~1), (*where P is*

186 *pressure of N_2 gas in the adsorption system and P_0 is N_2 gas saturation pressure at 77 K*)

187 was used to determine the total pore volume of the biochars (Hagemann et al., 2017).

2.7. Spectroscopic analysis of biochars

An X-ray diffractometer (X'pert Pro, Netherlands) fitted with a Ni foil filter and CuKα radiation for crystalline phase identification was used to record the X-Ray diffraction pattern and crystalline formation on the biochars. The x-ray tube was energized at 40 kV and 40 mA and samples were scanned from an angle (2θ) of 5° to 90° using a step size of 0.026° (2θ) and a scan speed of $1.0°$ min^{-1} (Singh et al., 2017). The elemental composition of biochars (pre- and post-adsorption biochars) at the outermost 10 nm of the surfaces was analysed using ESCALAB 250Xi X-ray Photoelectron Spectrometer (XPS) equipped with monochromated Al K α (1486.68 eV, 150 W). The bonding behavior of organic functional groups (often scattered on the surface of biochars), was measured using the Thermo Scientific Nicolet FT-IR spectrometer (Nicolet 8700). To do this, the biochar samples were prepared in pellets of fused KBr and 32 scans were made within the $4000 - 400$ cm^{-1} regions.

3. Results and Discussion

### 3.1. As(III) removal from solution without biochar

Arsenite was removed from solution through the formation of solid precipitates when solutions of $NaAsO_2$ and $CaCl_2$ were equilibrated at 25 ^oC with and without biochar. Previous reports (e.g. Jung et al., 2018; Renard et al., 2015) have also suggested the precipitation of Ca-As derivatives (i.e. calcium arsenites or calcium arsenates) as a mechanism for the removal of arsenic in water. X-Ray diffraction (XRD) analysis of the solid precipitates revealed the presence of crystalline calcium arsenite and Portlandite (i.e. $Ca(AsO_2)_2$ and $Ca(OH)_2$) occurring mainly around $2\theta = 10.1^o$ and 28.8^o respectively (Fig. 1). Calcium arsenate was also precipitated as revealed by peaks around $2\theta = 30.9°$ (Fig 1) corresponding to Johnbaumite ($Ca_5(AsO_4)_3OH$). Calcium arsenate was unexpected given that only As(III) was added in solution during the experimental procedure. However, the occurrence of calcium arsenate could be attributed to the rapid oxidation of some As(III) to

213   As(V) by chloride ions from the $CaCl_2$ used in the study as the source of Ca. This mirrors

214   the results of Ahmad et al. (2020), Alam et al. (2018) and Hu et al. (2012) suggesting that

215   chemicals such as chlorine, ozone and permanganate rapidly oxidize As(III) to the less toxic

216   and easy to remove As(V) at pH levels less than 8.3.

3.1.1. Effects of pH on As(III) removal

218   The quantity of As(III) removed by precipitation from the solution was significantly affected

219   by solution pH. At pH 4.5, precipitation was low and only 4.1 % of As(III) was removed

220   from solution at equilibrium (Fig. 2a). At this low pH, H_3AsO_3 species predominate in

221   aqueous solution and the sorption ability of H_3AsO_3 is weaker than water (Roman-Ross et

222   al., 2006), leading to low sorption of As(III). This may explain why XRD analysis indicated

223   only few peaks at pH 4.5 (Fig. 1). At pH 6.5, more peaks with greater intensity were seen on

224   the XRD spectrum corresponding mainly to calcium arsenite, calcite and Johnbaumite (Fig

225   1). At this pH level, 25.4 % of As(III) was removed from solution (Fig. 2a). This results are

226   consistent with the findings of Zhu et al. (2006) who suggested that at circumneutral pH

227   conditions, Ca-As precipitates become increasingly stable as arsenite species often exists at

228   neutral state ($As(OH)_3^o$). According to Roman-Ross et al. (2006), up to 98 % of this neutral

229   arsenite species is often present in solution between pH 6.5 to pH 7.5 and the sorption of this

230   non-ionic species on a neutral, or slightly positively charged ionic surface is encouraged,

231   leading to significant increases in sorption beyond a monolayer (eqn. 6). This may explain

232   why As(III) removal was significantly higher at pH 6.5.

233    $$Ca^{2+} + H_3AsO_3^o = CaHAsO_3(s) + 2H^+ \qquad\qquad (6)$$
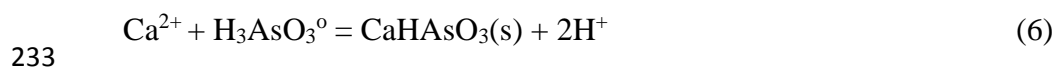
234   As pH conditions increased to 9.5, the stability of the precipitates appeared to decrease as

235   arsenite species become negatively charged and behave like a weak acid. At this pH level,

236   the precipitation of calcium carbonate (eqn. 7) predominates the chemical reaction. Sumathi

10

237 & Alagumuthu, (2014) also noted that increasing concentrations of OH⁻ at high pH values

238 reverses the arsenite sorption process and the formation of competitive OH⁻ plays an

239 important role leaving behind arsenic in the aqueous solution. This may also explain why

240 fewer and weaker peaks were detected at pH 9.5 (Fig. 1) and only 0.91 % of As (III) was

241 removed from solution (Fig. 2a).

$$Ca^{2+} + H_2CO_{3\,(aq)} = CaCO_3(s) + 2H^+ \qquad\qquad (7)$$

242
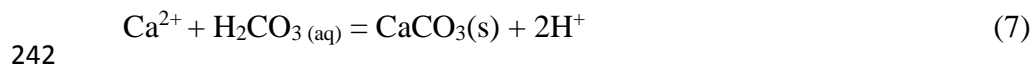
3.1.2. Effects of biochar addition on As(III) removal

244 Biochar addition had varying effects on the amount of As(III) removed through precipitation

245 and this was strongly dependent not only on biochar type but also solution pH as explained

246 in section 3.1.1. Under acidic conditions (pH 4.5), the addition of rice husk biochar (i.e. RB4

247 and RB7) did not influence As(III) removal and there was no net reduction in the

248 concentration of As(III) in solution. Instead, the concentration of As(III) in solution slightly

249 increased by 0.9 % and 0.6 %, for RB4 and RB7 respectively (Fig. 2b). This slight increase

250 in As(III) concentration may have resulted from the inherent arsenic content of the rice husk

251 biochar (Table 1). Wood biochar (i.e. WB4 and WB7) on the other hand was slightly

252 beneficial at pH 4.5, decreasing As(III) concentration in solution by 11.4 % and 14.6 %,

253 respectively (Fig. 2b). XRD analysis (Fig.3a) revealed a low intensity peak at $2\theta = 30.9°$ on

254 wood biochars (i.e. WB4c and WB7c) corresponding to the crystalline phase of

255 Johnbaumite.

256 At pH 6.5, the removal of As(III) was significantly higher (i.e. 19.3, 22.5, 54.0 and 58.1 %),

257 when all four biochars were added (i.e. RB4, RB7, WB4 and WB7 respectively) (Fig. 2b).

258 Compared to the treatments without biochar which removed a maximum of 25.4 % of As(III)

259 from solution, the addition of biochar (especially wood biochar), doubled the removal of

260 As(III) from solution by 54.0 % and 58.1 % for WB4 and WB7 respectively, indicating that

11

261   biochar addition significantly aided the precipitation process at pH 6.5. XRD analysis

262   revealed stronger peaks on wood biochar occurring around $2\theta = 28.8°$, $30.1°$ and $30.9°$, all

263   corresponding to crystalline phases of calcium arsenites and arsenates (i.e. $Ca(AsO_2)_2$,

264    $CaAsO_2OH \cdot \frac{1}{2}H_2O$, and $Ca_5(AsO_4)_3OH$) (Fig. 3b). Rice husk biochar did not return any

265   noticeable peaks.

266   All biochars (RB4, RB7, WB4 and WB7) added under alkaline conditions (pH = 9.5) were

267   counter-productive as their addition slightly increased the concentration of arsenic in

268   solution by 5.3, 4.7, 2.6, and 2.0 % respectively (Fig. 2b). A slight increase in arsenic

269   concentration in solution following the addition of biochar could be attributed to the

270   increased conversion of precipitated Ca-As compounds to calcium carbonate (in the presence

271   of atmospheric CO_2), which in turn released the arsenic back into solution (Korchef, and

272   Touaibi, 2020). This may happen when arsenic species become increasingly negative at

273   higher pH conditions and competition for sorption sites between arsenic species and

274   carbonates increases (Sø et al., 2008; Yokoyama et al., 2012). Tiwari and Pandey (2013) and

275   Beesley et al. (2013) also explained that arsenic may be re-mobilized in solution at pH > 8

276   when OH$^-$ ions displace anionic arsenic (AsO_3^{3-}) through electrostatic interactions. The

277   inherent content of arsenic in biochars (Table 1), may have also contributed to the slight

278   increase in arsenic concentration in solution under alkaline conditions. XRD analysis on the

279   post adsorption biochars at pH = 9.5, did not reveal any noticeable peaks, indicating that

280   crystalline structures were rare at this pH level (Fig. 3c).

281   Compared to the control treatments, the addition of biochar generally enhanced precipitation

282   that led to the increased removal of As(III) from solution. The possible reasons are two-fold:

283   Firstly, biochar with its large surface area and porosity offers an excellent structure for the

284   precipitation of calcium derivatives. This explains why wood biochar, which had a larger

285   surface area and pore size compared to rice husk biochar was more effective in enhancing

286   the removal of As(III) from solution. Precipitates occurring deep inside the pores of the

287   biochar may have been trapped, and "locked away", by those formed near the surface of the

288   biochar, especially at pH 6.5, where precipitates were more stable. The locking away of these

289   precipitates containing As(III) reduced their chances of dissolution and therefore resulted to

290   the significant reduction of As(III) concentration in solutions when biochar was added.

291   Secondly, the inherent content of Ca in the biochars (especially the wood biochars) may have

292   played a key role in increasing the amount of Ca ions involved in the precipitation process.

293   This may also explain why wood biochar, with higher Ca content (i.e. 98.2 and 110 mgkg^{-1}

294   for WB4 and WB7 respectively) compared to rice husk biochar (i.e. 3.38 and 2.91 mgkg^{-1}

295   for RB4 and RB7 respectively), was more effective in removing As(III) from solution.

296   **3.2.Sorption isotherms and thermodynamic analysis**

297   Two sorption models (Langmuir and Freundlich models) were tested to explain the sorption

298   behavior of As(III) on all four biochars. Based on the correlation coefficient (R^2) values of

299   the two sorption models, the Freundlich sorption model, with higher R^2 values (Table 2),

300   could best explain the sorption behavior of As(III) on all the biochars. This was an indication

301   that As(III) sorption on the biochars was characterized by heterogeneous multilayer sorption

302   with a distribution of sorption sites of different characteristic energies. The 'n' values were

303   greater than unity (n > 1) (Table 2), implying that it was chemisorption and the isotherm was

304   L-type with a high affinity between As(III) and the biochars (Sumathi and Alagumuthu,

305   2014).

306   Thermodynamic parameters obtained from all four biochars indicated that change in free

307   energy (Δ**G**º) was negative for all four biochars and decreased with increasing temperatures

308   (Table 3). This was an indication that the sorption process of As(III) on all four biochars was

309   feasible and spontaneous. The negativity of Δ**G**º increased with increasing temperatures

310   from 298 to 318 K (Table 3), indicating that the sorption process was more favorable at

311   higher temperatures. In addition, the change in enthalpy (ΔH^o) and entropy (ΔS^o) were

312   positive for all biochars (Table 3), indicating that the sorption process was endothermic with

313   more randomness at the solid-solution interface.

3.3. Arsenic desorption and effects of pH

315   Desorption experiments were used to assess the stability of sorbed arsenic on the biochars

316   over a wide range of pH levels. All four biochars (RB4, RB7, WB4 and WB7) were used

317   and the pH was varied at 4.5, 6.5, and 9.5. Arsenic was more stable on wood biochar than

318   rice husk biochar especially at pH 6.5 (Fig. 4). Comparatively, only small quantities of

319   arsenic (i.e. 0.03 % and 0.33 %) were released into solution after the desorption test on WB4

320   and WB7 respectively. This could be attributed in part, to wood biochar's high porosity and

321   large surface area that was able to retain Ca-As precipitates and prevent them from

322   dissolution. Desorption on rice husk biochar at pH 9.5, was significantly high (11.6 and 10.4

323   % on RB4 and RB7 respectively) compared to desorption on wood biochar (2.00 and 1.28

324   % on WB4 and WB7 respectively) at the same pH level. As explained earlier, this

325   phenomenon could be attributed to the ability of wood biochar to retain precipitates.

3.4. The effects of biochar properties on As(III) removal

3.4.1. Biochar porosity

328   FE-SEM images of wood-based biochars revealed the occurrence of micro and macro sized

329   pores that were likely sites for the retention of Ca-As precipitates (Fig. 5a). The SEM images

330   showed precipitates occuring in aggregates in the pores of the biochars (Fig. 5b) and EDX

331   analysis indicated higher Ca/As ratios of 1 and 1.5 in these regions (Fig. 5c) corresponding

332   to Ca-As derivatives such as $Ca(AsO_2)_2$, $CaAsO_2OH \cdot \frac{1}{2}H_2O$ and $Ca_5(AsO_4)_3OH$. In another

333   study, Marshall et al. (2017) suggested that such precipitates were held in place by

334   electrostatic attractions between calcium cations and oxygen containing functional groups

14

335 (anions). In their study using phosphorus (chemical analogue of arsenic), they observed the

336 formation of phosphate aggregates on the surface of biochar and calcium adsorbed onto the

337 edges of short range ordered graphitic sheets through ionic interactions with oxygen

338 containing functional groups on the biochar. The calcium sites were able to clog phosphate

339 onto the edges of the graphitic sheet making biochar to act as seed material for the formation

340 of calcium phosphates (Marshall et al., 2017).

341 Porosity in rice husk biochar was poor (Fig. 6a), implying that rice husk biochar had a

342 slightly lower ability to trap and retain precipitates compared to the wood biochar. This may

343 explain why rice husk biochar had a slighly lower ability to retain sorbed As(III). EDX

344 analysis on the rice husk biochars indicated high quantities of silicon (Fig. 5b) and

345 insignificant quantities of calcium and arsenic species.

346 **3.4.2. Pyrolysis temperature**

347 As expected, pyrolysis temperature significantly affected the basic properties of biochar such

348 as elemental contents, functional groups and biochar surface area and porosity. Increase in

349 temperatures increased the carbon content of biochars, which was significantly higher in

350 wood biochar (78.4 % and 91.0 % for WB4 and WB7, respectively) than rice husk biochar

351 (49.2 % and 51.0 % for RB4 and RB7, respectively) (Table 1). Differences in carbon content

352 was due to differences in lignocellulosic content and higher aromatic carbon in wood

353 (McBeath et al., 2014; Zama et al., 2017). Biochar yield decreased with increasing pyrolysis

354 temperature (Table 1) due to increasing degradation of lignocellulosic materials at high

355 temperatures and the removal of most volatile components (Chowdhury, et al., 2016;

356 Figueiredo et al., 2017; Novak et al., 2014). There was a significant decrease in the H:C

357 atomic ratio with increasing pyrolysis temperature especially in wood biochars signifying an

358 increase in carbonization and dehydration as pyrolysis temperature increased (Yuan et al.,

359 2015; Alkurdi et al., 2020). Similarly, there was a significant decrease in the O:C and

15

360 (O+N):C atomic ratios with increase in pyrolysis temperature in wood biochars indicating

361 increased aromaticity and polarity with increase in temperature (Zhao et al., 2017). Wood

362 biochar had a significantly higher BET surface area (125 and 308 m^2 g^{-1} for WB4 and WB7,

363 respectively) compared to rice husk biochar (110 and 247 m^2 g^{-1} for RB4 and RB7,

364 respectively). Surface areas increased with increasing pyrolysis temperature possibly due to

365 increasing pore sizes.

366 ### 3.4.3. XPS analysis

367 X-ray photoelectron spectroscopy (XPS) was used to study the surface chemistry of the

368 biochars before and after adsorption. The XPS data was deconvulated and C1s scan of WB4

369 revealed the presence of C-H, C-C and C=C bonds stretching at a binding energy of 284.5

370 eV (Fig. 7a). Other functional groups (C-O-C and C-O) also occurred on WB4 at a binding

371 energy of 285.8 eV. After adsorption, the peak at 284.5 eV shifted to 284.6 eV on WB4c

372 and the peak at 285.8 eV shifted to 285.7 eV on WB4c (Fig. 7b). A new peak on WB4c was

373 observed at a binding energy of 288.3 eV corresponding to O-C=O stretching but the

374 intensity was very low (Fig. 7b). $CaCO_3$ was also detected on WB4 at a binding energy of

375 347.2 eV when Ca2p scans were deconvolated (Fig. 7c). This peak increased in intensity on

376 the post-adsorption biochar (WB4c) and slighly shifted from 347.2 to 347.1 eV (Fig. 7d) with

377 no effects on the bond constitution. A new peak also appeared at 351.6 eV on WB4c (Fig.

378 7d) indicating an interaction between Ca and a metal; possibly As. The occurrence of trace

379 amounts of As (due to inherent arsenic) was noticed on WB4 at a binding energy of 44.7 eV

380 (Fig. 7e) which significantly shifted with greater intensity to 45.1 eV on WB4c (Fig. 7f)

381 indicating an increase in the concentration of As on the post-equilibrium biochars.

382 ### 3.4.4. FTIR analysis

383 As expected, biochars made at lower temperatures (i.e. WB4 and RB4) had a higher

384 abundance of functional groups (e.g. O-H, C-H, C=H and C=O) compared to biochars made

16

385 at higher temperatures (WB7 and RB7) (Fig. 8a). Previous reports have attributed this

386 phenomenon to the thermal decomposition of most functional groups at higher temperatures

387 (Tomczyk et al., 2020; Chatterjee et al., 2020). As pyrolysis temperature increases,

388 dehydration, decarbonylation and decarboxylation reactions take place and poly-condensed

389 aromatic structures are formed and poly-aromatization becomes dominant (McBeath et al.,

390 2014). Increasing dehydration and carbonization led to the loss of hydroxyl (O-H) as well as

391 aliphatic and asymmetric C-H functional groups on WB7 and RB7, which usually occur at

392 wavelengths around 3200 and 2900 cm^{-1} respectively. Aromatic species involving C=C ring

393 stretching of benzene derivatives and C=O stretching of conjugated ketones and quinones

394 (Chowdhury et al., 2016; Zhao et al., 2017), occurred between 1600 cm^{-1} and 1400 cm^{-1} on

395 the lower temperature biochars (WB4 and RB4). These species also became fewer at higher

396 temperatures (700 °C) as carbonization and aromaticity increased. Increase in aromaticity

397 and the occurrence of out–of-plane deformation by aromatic C–H groups occurring between

398 750 to 890 cm^{-1} was likely due to the degradation and depolymerization of cellulose,

399 hemicelluloses and lignin especially as pyrolysis temperature increased (Zhao et al., 2017).

400 Polar functional group composition on post-adsorption biochars showed minimal differences

401 in abundance compared to pre-adsorption biochars at pH 6.5 (Fig. 8b). There were however,

402 major peak shifts (e.g. O-H vibrations shifting from 3340 on the pre adsorption biochars to

403 3259 on the post adsorption biochars) (Fig. 8b), probably due to interactions with added

404 experimental species of calcium and arsenic. Major functional groups such as C=C and C=O

405 also became fewer on the post adsorption biochars.

406 **4. Conclusions**

407 It has been demonstrated that As pollution can be reduced through arsenic precipitation with

408 calcium compounds (e.g. CaO and CaCl$_2$). This study was aimed at enhancing the

409 precipitation process using unmodified biochar, made from rice husk (RB) and aspen wood

410 (WB) at 400 °C and 700 °C. The addition of biochar was beneficial at pH 6.5, where arsenic

411 sorption and Ca/As precipitation removed up to 58.1 % of As(III) on wood biochars

412 compared to 25.4 % in solutions without biochar (controls). Calcium arsenite and arsenate

413 species precipitated and deposited as aggregates in the pores of biochars were $Ca(AsO_2)_2$,

414 $CaAsO_2OH \cdot \frac{1}{2}H_2O$ and $Ca_5(AsO_4)_3OH$. Wood biochars (i.e. WB4 and WB7) were better at

415 retaining precipitates with a desorption rate of 0.1 % and 0.3 % respectively compared to

416 rice husk biochars (RB4 and RB7) with desorption rates of 3.2 % and 2.9 % respectively at

417 pH 6.5. Overall, near neutral pH conditions were favorable for the precipitation process as

418 well as retarding the dissolution of precipitates formed. The results demonstrated that

419 biochar, without the need for modification, can be successfully used to enhance Ca/As

420 precipitation, leading to increased removal of As(III) from solution.

421 **Acknowledgements**

426

427

428

429

430

431

432

433 **References**

434 Ahmad, A., Heijnen, L., de Waal, L., Battaglia-Brunet, F., Oorthuizen, W., Pieterse, B.,

435   Bhattacharya, P. and van der Wal, A., (2020). Mobility and redox transformation of

436   arsenic during treatment of artificially recharged groundwater for drinking water

437   production. *Water Research*, p.115826.

438 Agrafioti, E., Kalderis, D., & Diamadopoulos, E. (2014). Ca and Fe modified biochars as

439   adsorbents of arsenic and chromium in aqueous solutions. *Journal of Environmental*

440   *Management, 146*, 444-450.

441 Alam, M.A., Shaikh, W.A., Alam, M.O., Bhattacharya, T., Chakraborty, S., Show, B. and

442   Saha, I., (2018). Adsorption of As (III) and As (V) from aqueous solution by

443   modified Cassia fistula (golden shower) biochar. Applied Water Science, 8(7), p.198.

444 Alkurdi, S. S., Al-Juboori, R. A., Bundschuh, J., Bowtell, L., & McKnight, S. (2020). Effect

445   of pyrolysis conditions on bone char characterization and its ability for arsenic and

446   fluoride removal. Environmental Pollution, 262, 114221.

447 Beesley, L., Marmiroli, M., Pagano, L., Pigoni, V., Fellet, G., Fresno, T., Vamerali, T.,

448   Bandiera, M., Marmiroli, N. (2013). Biochar addition to an arsenic contaminated

449   soil increases arsenic concentrations in the pore water but reduces uptake to tomato

450   plants (*Solanum lycopersicum* L.). *Science of the Total Environment, 454*, 598-603.

451 Chatterjee, R., Sajjadi, B., Chen, W.Y., Mattern, D.L., Hammer, N., Raman, V. and Dorris,

452   A., (2020). Effect of Pyrolysis Temperature on Physico-Chemical Properties and

453   Acoustic-Based Amination of Biochar for Efficient CO2 Adsorption. *Frontiers in*

454   *Energy Research*, 8, p.85.

455 Chowdhury, Z. Z., Karim, M. Z., Ashraf, M. A., & Khalid, K. (2016). Influence of

456   carbonization temperature on physicochemical properties of biochar derived from

457   slow pyrolysis of durian wood (*Durio zibethinus*) sawdust. *BioResources, 11*(2),

458   3356-3372.

459   Deng, Y., Weng, L., Li, Y., Chen, Y., & Ma, J. (2020). Redox-dependent effects of

460   phosphate on arsenic speciation in paddy soils. Environmental Pollution, 264,

461   114783.

462   Figueiredo, C., Lopes, H., Coser, T., Vale, A., Busato, J., Aguiar, N., Novotny, E., Canellas,

463   L. (2017). Influence of pyrolysis temperature on chemical and physical properties of

464   biochar from sewage sludge. *Archives of Agronomy and Soil Science*, 1-9.

465   Guan, X., Ma, J., Dong, H., & Jiang, L. (2009). Removal of arsenic from water: effect of

466   calcium ions on As(III) removal in the $KMnO_4$–Fe(II) process. *Water Research,*

467   *43*(20), 5119-5128.

468   Hagemann, N., Joseph, S., Schmidt, H.-P., Kammann, C. I., Harter, J., Borch, T., Young,

469   R.B., Varga, K., Taherymoosavi, S., Elliott, K. W. (2017). Organic coating on

470   biochar explains its nutrient retention and stimulation of soil fertility. *Nature*

471   *Communications, 8*(1), 1089.

472   He, R., Peng, Z., Lyu, H., Huang, H., Nan, Q., & Tang, J. (2018). Synthesis and

473   characterization of an iron-impregnated biochar for aqueous arsenic removal.

474   *Science of the Total Environment, 612*, 1177-1186.

475   Hong, Y. S., Song, K. H., & Chung, J. Y. (2014). Health effects of chronic arsenic exposure.

476   *Journal of Preventive Medicine and Public Health*, *47*(5), 245.

477   Hu, C., Liu, H., Chen, G., Jefferson, W.A. and Qu, J., (2012). As (III) oxidation by active

478   chlorine and subsequent removal of As (V) by Al_{13} polymer coagulation using a

479   novel dual function reagent. *Environmental science & technology*, 46(12), 6776-

480   6782.

481 Hu, X., Ding, Z., Zimmerman, A. R., Wang, S., & Gao, B. (2015). Batch and column

482   sorption of arsenic onto iron-impregnated biochar synthesized through hydrolysis.

483   *Water Research, 68*, 206-216.

484 Huq, M. E., Su, C., Fahad, S., Li, J., Sarven, M. S., & Liu, R. (2018). Distribution and

485   hydrogeochemical behavior of arsenic enriched groundwater in the sedimentary

486   aquifer comparison between Datong Basin (China) and Kushtia District

487   (Bangladesh). *Environmental Science and Pollution Research*, 25(16), 15830–15843

488 Jung, B., Safan, A., Duan, Y., Kaushik, V., Batchelor, B. and Abdel-Wahab, A., (2018).

489   Removal of arsenite by reductive precipitation in dithionite solution activated by UV

490   light. *Journal of Environmental Sciences*, 74, pp.168-176.

491 Korchef, A. and Touaibi, M., (2020). Effect of pH and temperature on calcium carbonate

492   precipitation by CO2 removal from iron-rich water. W*ater and Environment Journal*,

493   34(3), pp.331-341.

494 Kurniawan, T. A., Chan, G. Y., Lo, W.-H., & Babel, S. (2006). Comparisons of low-cost

495   adsorbents for treating wastewaters laden with heavy metals. *Science of the Total*

496   *Environment, 366*(2-3), 409-426.

497 Lin, L., Qiu, W., Wang, D., Huang, Q., Song, Z., & Chau, H. W. (2017). Arsenic removal

498   in aqueous solution by a novel Fe-Mn modified biochar composite: Characterization

499   and mechanism. *Ecotoxicology and Environmental Safety, 144*, 514-521.

500 Marshall, J. A., Morton, B. J., Muhlack, R., Chittleborough, D., & Kwong, C. W. (2017).

501   Recovery of phosphate from calcium-containing aqueous solution resulting from

502   biochar-induced calcium phosphate precipitation. *Journal of Cleaner Production,*

503   *165*, 27-35.

504 Martínez-Villegas, N., Briones-Gallardo, R., Ramos-Leal, J. A., Avalos-Borja, M.,

505   Castañón-Sandoval, A. D., Razo-Flores, E., & Villalobos, M. (2013). Arsenic

506   mobility controlled by solid calcium arsenates: A case study in Mexico showcasing

507   a potentially widespread environmental problem. Environmental Pollution, 176, 114-

508   122.

509 McBeath, A. V., Smernik, R. J., Krull, E. S., & Lehmann, J. (2014). The influence of

510   feedstock and production temperature on biochar carbon chemistry: a solid-state ^{13}C

511   NMR study. *Biomass and Bioenergy, 60*, 121-129.

512 Mudhoo, A., Sharma, S. K., Garg, V. K., & Tseng, C.-H. (2011). Arsenic: an overview of

513   applications, health, and environmental concerns and removal processes. *Critical*

514   *Reviews in Environmental Science and Technology, 41*(5), 435-519.

515 Novak, J. M., Cantrell, K. B., Watts, D. W., Busscher, W. J., & Johnson, M. G. (2014).

516   Designing relevant biochars as soil amendments using lignocellulosic-based and

517   manure-based feedstocks. *Journal of Soils and Sediments, 14*(2), 330-343.

518 Renard, F., Putnis, C. V., Montes-Hernandez, G., Ruiz-Agudo, E., Hovelmann, J., & Sarret,

519   G. (2015). Interactions of arsenic with calcite surfaces revealed by in situ nanoscale

520   imaging. *Geochimica et Cosmochimica Acta, 159*, 61-79.

521 Roman-Ross, G., Cuello, G. J., Turrillas, X., Fernandez-Martinez, A., & Charlet, L. (2006).

522   Arsenite sorption and co-precipitation with calcite. Chemical geology, 233(3-4), 328-

523   336.

524 Shankar, S. and Shanker, U., (2014). Arsenic contamination of groundwater: a review of

525   sources, prevalence, health risks, and strategies for mitigation. The Scientific World

526   Journal, 2014.

527 Singh, B., Camps-Arbestain, M., & Lehmann, J. (2017). *Biochar: a guide to analytical*

528   *methods*: Csiro Publishing.

529   Sø, H.U., Postma, D., Jakobsen, R. and Larsen, F., (2008). Sorption and desorption of

530   arsenate and arsenite on calcite. Geochimica et Cosmochimica Acta, 72(24),

531   pp.5871-5884.

532   Sumathi, T., & Alagumuthu, G. (2014). Adsorption studies for arsenic removal using

533   activated Moringa oleifera. International Journal of Chemical Engineering, 2014.

534   Tchounwou, P. B., Yedjou, C. G., Patlolla, A. K., & Sutton, D. J. (2012). Heavy metal

535   toxicity and the environment *Molecular, Clinical and Environmental Toxicology* (pp.

536   133-164): Springer.

537   Tiwari, S., & Pandey, V. (2013). Removal of arsenic from drinking water by precipitation

538   and adsorption or cementation: An environmental prospective. *Recent Research in*

539   *Science and Technology, 5*(5).

540   Tomczyk, A., Sokołowska, Z., & Boguta, P. (2020). Biochar physicochemical properties:

541   pyrolysis temperature and feedstock kind effects. Reviews in Environmental Science

542   and Bio/Technology, 1-25.

543   Wu, C., Huang, L., Xue, S.-G., Huang, Y.-Y., Hartley, W., Cui, M.-Q., & Wong, M.-H.

544   (2017). Arsenic sorption by red mud-modified biochar produced from rice straw.

545   *Environmental Science and Pollution Research, 24*(22), 18168-18178.

546   Yokoyama, Y., Mitsunobu, S., Tanaka, K., Itai, T., & Takahashi, Y. (2009). A study on the

547   coprecipitation of arsenite and arsenate into calcite coupled with the determination

548   of oxidation states of arsenic both in calcite and water. Chemistry letters, 38(9), 910-

549   911.

550   Yokoyama, Y., Tanaka, K., & Takahashi, Y. (2012). Differences in the immobilization of

551   arsenite and arsenate by calcite. *Geochimica et Cosmochimica Acta, 91*, 202-219.

552 Yousaf, B., Liu, G., Abbas, Q., Wang, R., Ali, M. U., Ullah, H., Liu, R., Zhou, C. (2017).

553 Systematic investigation on combustion characteristics and emission-reduction

554 mechanism of potentially toxic elements in biomass-and biochar-coal co-combustion

555 systems. *Applied Energy, 208*, 142-157.

556 Yuan, H., Lu, T., Huang, H., Zhao, D., Kobayashi, N., & Chen, Y. (2015). Influence of

557 pyrolysis temperature on physical and chemical properties of biochar made from

558 sewage sludge. *Journal of Analytical and Applied Pyrolysis, 112*, 284-289.

559 Zama, E.F., Zhu, Y.G., Reid, B.J. and Sun, G.X., (2017). The role of biochar properties in

560 influencing the sorption and desorption of Pb (II), Cd (II) and As (III) in aqueous

561 solution. Journal of cleaner production, 148, pp.127-136.

562 Zama, E.F., Reid, B.J., Sun, G.X., Yuan, H.Y., Li, X.M. and Zhu, Y.G., (2018). Silicon (Si)

563 biochar for the mitigation of arsenic (As) bioaccumulation in spinach (Spinacia

564 oleracean) and improvement in the plant growth. Journal of Cleaner Production, 189,

565 pp.386-395.

566 Zhang, C., Liu, L., Zhao, M., Rong, H. and Xu, Y., (2018). The environmental characteristics

567 and applications of biochar. Environmental Science and Pollution Research, 25(22),

568 pp.21525-21534.

569 Zhao, S.-X., Ta, N., & Wang, X.-D. (2017). Effect of Temperature on the Structural and

570 Physicochemical properties of biochar with apple tree branches as feedstock

571 material. *Energies, 10*(9), 1293.

572 Zheng, R., Chen, Z., Cai, C., Tie, B., Liu, X., Reid, B. J., Huang, Q., Lei, M., Sun, G.,

573 Baltrėnaitė, E. (2015). Mitigating heavy metal accumulation into rice (*Oryza sativa*

574 L.) using biochar amendment—a field experiment in Hunan, China. *Environmental*

575 *Science and Pollution Research, 22*(14), 11097-11108.

576   Zhu, Y., Zhang, X., Xie, Q., Wang, D., & Cheng, G. (2006). Solubility and Stability of

577   Calcium Arsenates at 25°C. *Water, Air, and Soil Pollution, 169*(1-4), 221-238.

578

579

580

581

582

583

584

585

586

587

588

589

590

591

592

593

594

595

596   **Tables and figures legend**

597   **TABLES**

598   **Table 1:** Physical and chemical properties of biochars

599   **Table 2:** Sorption isotherm parameters for the sorption of As(III) on biochars

600   **Table 3:** Thermodynamic parameters of As(III) sorption on biochars

601

602   **FIGURES**

603   **Figure 1:** XRD analysis of precipitates formed in solutions without biochar at pH 4.5, 6.5

604   and 9.5.

605   **Figure 2:** The percentage removal of As(III) from solutions without biochar added (2a) and

606   with biochar added (2b) at pH 4.5, 6.5 and 9.5. Negative values indicate an increase in As

607   content in the solution.

608   **Figure 3:** XRD analysis of post-equilibrium biochars at pH = 4.5, 6.5 and 9.5.

609   **Figure 4**: The stability of Ca-As precipitates on biochar measured by the rate of arsenic

610   desorption into solution

611   **Figure 5:** FE-SEM analysis of biochar indicating porosity and aggregated structure of

612   precipitates formed in the pores of post-sorption biochars (5a and 5b). EDX analysis of

613   aggregates (5c)

614   **Figure 6:** SEM-EDX analysis of rice husk biochar indicating limited porosity and the

615   concentration of silicon.

616   **Figure 7:** XPS analysis of pre- and post-adsorption wood-based biochar (WB4 and WB4c).

617   Deconvulated C1s spectra of the biochars (7a and 7b), deconvulated Ca2p spectra of the

618   biochars (7c and 7d), deconvulated As3d scans of the biochars (7e and 7f).

619   **Figure 8:** FTIR analysis of pre-adsorption (8a) and post-adsorption (8b) biochars at pH 6.5.

620

621

622

623

Table 1

BC	C %	H %	N %	O %	Ca (mgkg⁻¹)	As (mgkg⁻¹)	C:N	H:C	O:C	(O+N)/C	Yield %	Ash %	BET surface area (m² g⁻¹)	Pore area (m² g⁻¹)	pH
RB4	49.2 ± 0.05	2.25 ± 0.8	0.50 ± 1.5	48.1 ± 0.2	3.38 ± 2.6	2.98 ± 5.3	116	0.55	0.73	0.74	56.7 ± 8.7	21 ± 3.0	110 ± 23	3.47 ± 9.1	9.49 ± 0.5
RB7	51.0 ± 0.5	0.3 ± 4.7	0.84 ± 1.9	47.8 ± 0.5	2.91 ± 4.3	2.22 ± 3.5	70.9	0.07	0.70	0.72	44.1 ± 12	32 ± 2.6	247 ± 19	108 ± 14	10.7 ± 0.01
WB4	78.4 ± 0.9	3.72 ± 9.1	0.41 ± 8.1	17.5 ± 1.2	98.2 ± 9.2	1.77 ± 0.3	223	0.57	0.17	0.17	39.9 ± 14	8.3 ± 5.3	125 ± 16	98.3 ± 13	9.78 ± 0.9
WB7	91.0 ± 0.7	1.03 ± 10	0.34 ± 6.5	7.64 ± 1.8	110 ± 6.3	2.06 ± 0.8	317	0.14	0.06	0.07	30.5 ± 11	11.4 ± 5.2	308 ± 11	132 ± 25	10.6 ± 0.55

28

624

625

626

627

628

629

630

Table 2

Biochar	Langmuir			Freundlich		
	R^2	Q_{max} (µg/g)	K_L	R^2	n	K_f (µg/g) (L/g)$^{1/n}$
RB4	0.932	3.265	0.321	**0.992**	1.67	0.401
RB7	0.846	2.601	0.301	**0.872**	1.64	0.921
WB4	0.803	6.856	0.094	**0.996**	2.54	1.110
WB7	0.871	5.254	0.088	**0.992**	2.40	0.909

Highlighted R^2 values indicate the model that best describes the sorption process of As(III) on biochars

631

632

633

634

635

636

637

638

639

640

641

642

643

644

645

646

647

648

649

650

651

Table 3

Biochar	T(K)	ΔG^o (KJ mol^{-1})	ΔH^o (KJ mol^{-1})	ΔS^o (J mol^{-1} K^{-1})
RB4	293	-1.98	20.16	31.14
	303	-2.21		
	318	-2.80		
RB7	293	-2.52	20.19	32.22
	303	-2.74		
	318	-2.98		
WB4	293	-5.05	36.42	79.14
	303	-5.72		
	318	-6.26		
WB7	293	-5.65	34.98	79.42
	303	-5.69		
	318	-5.99		

652

653

654

655

656

657

658

659

660

661

662

663

664

665

666

667

668

Figure 1

669

670

671

672

673

674

675

676

677

678

679

680

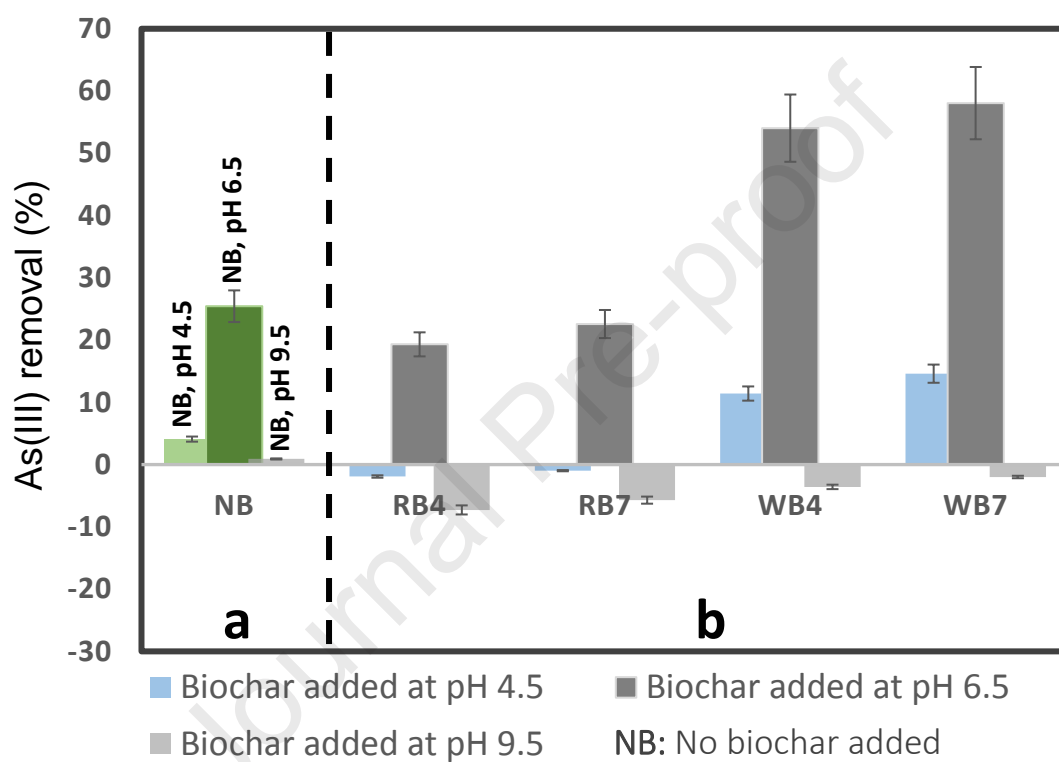681

682

683

684

685

686

687

688

689

690

691

692

693
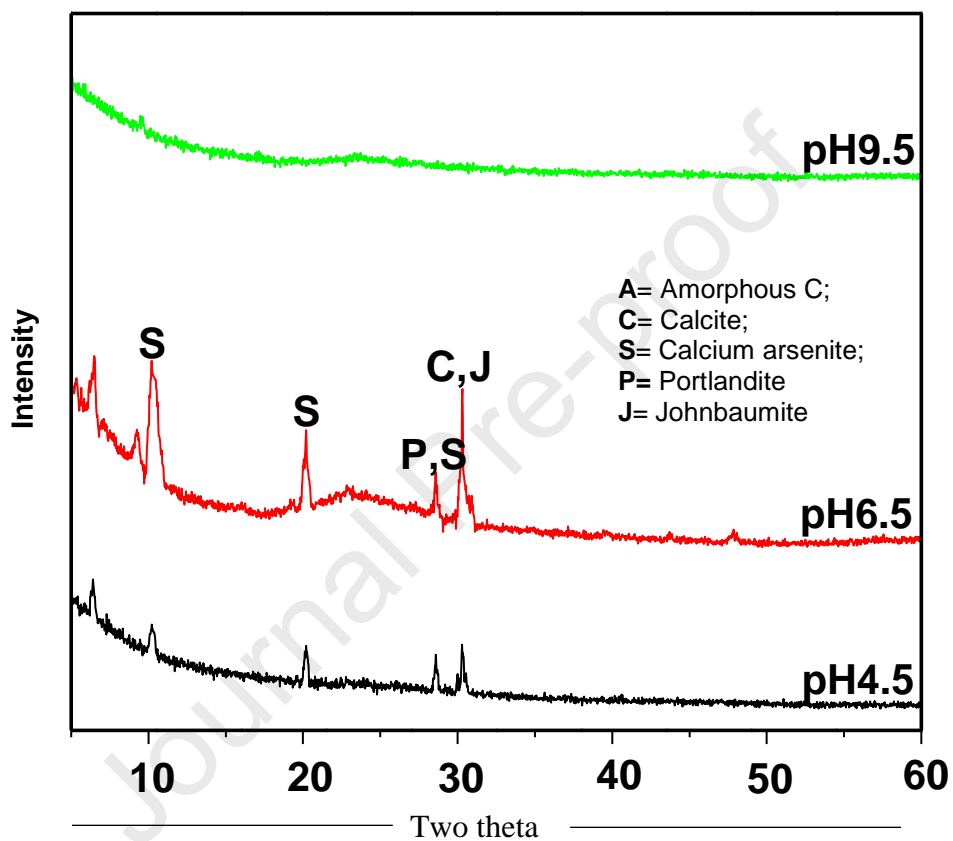
694

695

696

697

698

699

700 **Figure 2**

701

Figure 2. As(III) removal (%) for (a) NB (no biochar added) at pH 4.5, pH 6.5, and pH 9.5; and (b) RB4, RB7, WB4, WB7 with biochar added at pH 4.5, pH 6.5, and pH 9.5.

Legend:
- Biochar added at pH 4.5
- Biochar added at pH 6.5
- Biochar added at pH 9.5
- NB: No biochar added

725

726

727

728

729

730

731

732

733

734

735

736

737

738

739

740

741

742

743

744

745

746

747

748

749

750

751

752

753

754

755

Figure 3
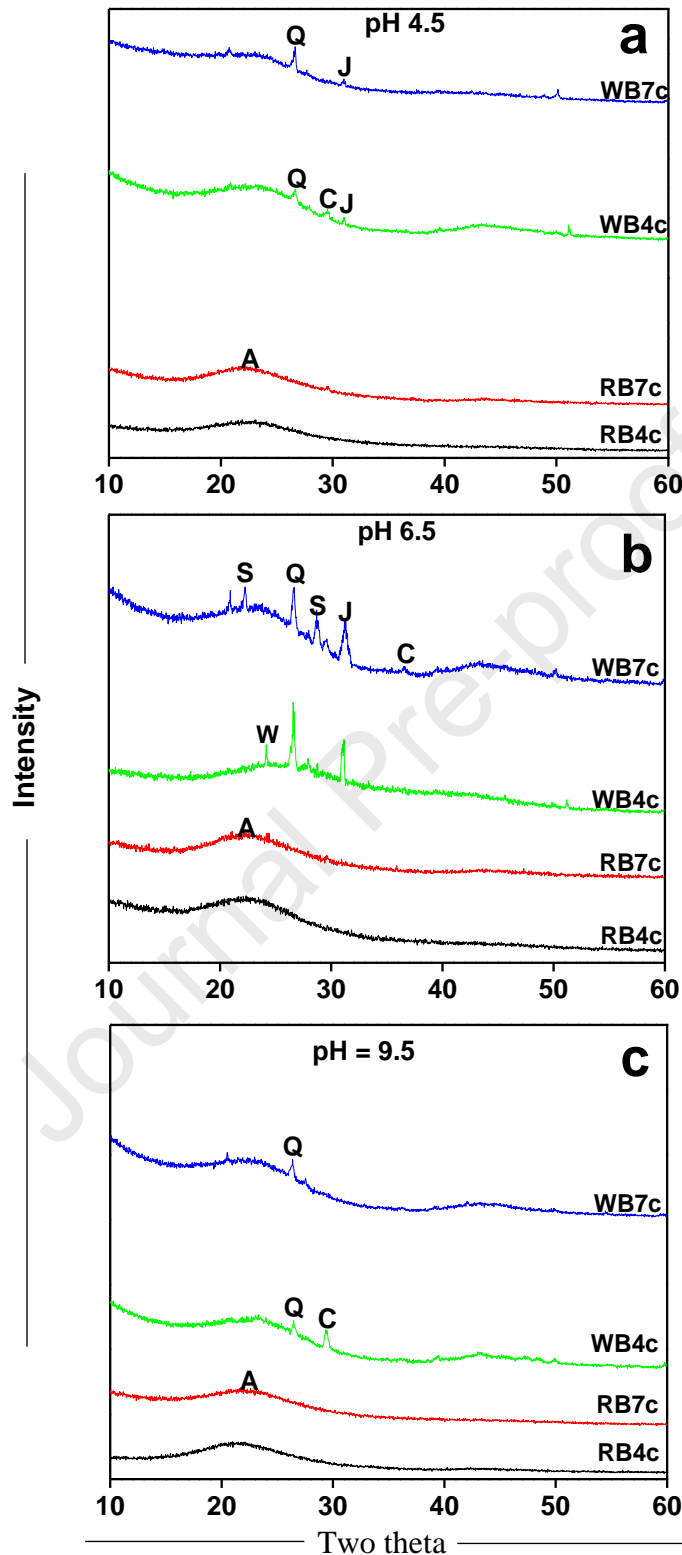
A, amorphous Si & C; **W**, Whewellite; **Q**, Quartz;

C, Calcite; **S**, Calcium arsenite; **J**, Johnbaumite

756

757

758

759

760

761

762 **Figure 4**

763

776 **pH**

777

778

779

780

781

782

783

784

785

786
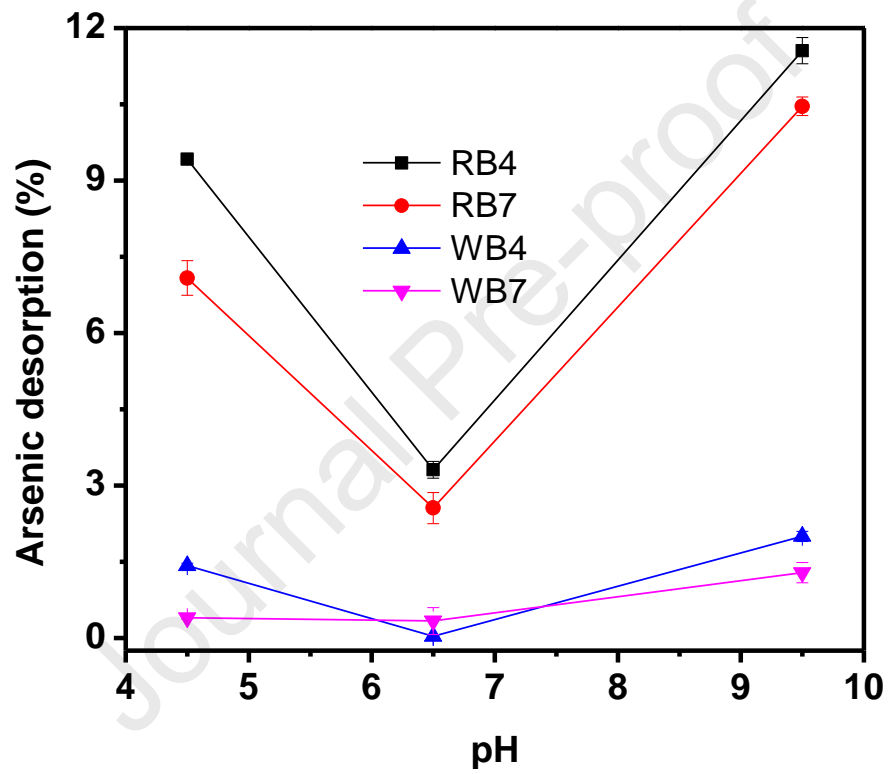
787

788

789

790

791

Figure 5

792

793

794

795

796

797

798

799

800

801

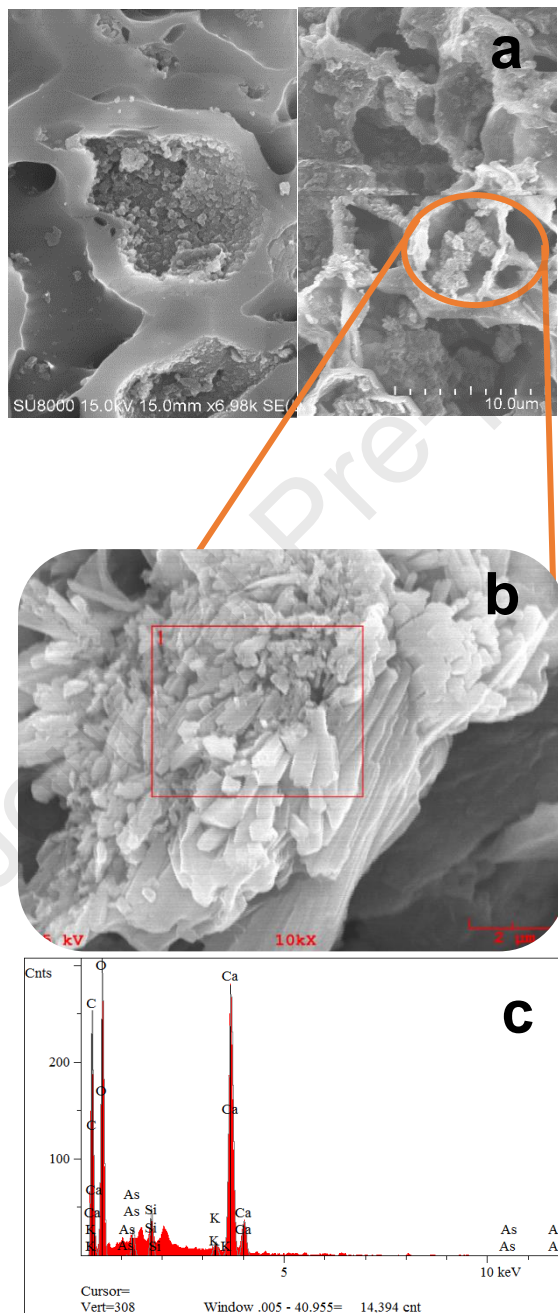802

803

804

805

806

807

808

809

810

811

812

813

814

815

816

817

35

818

819

820

821

822

823

824

825

826 **Figure 6**
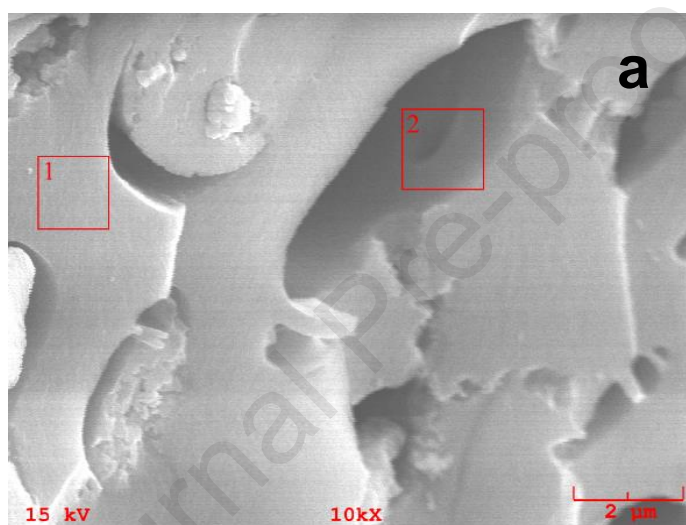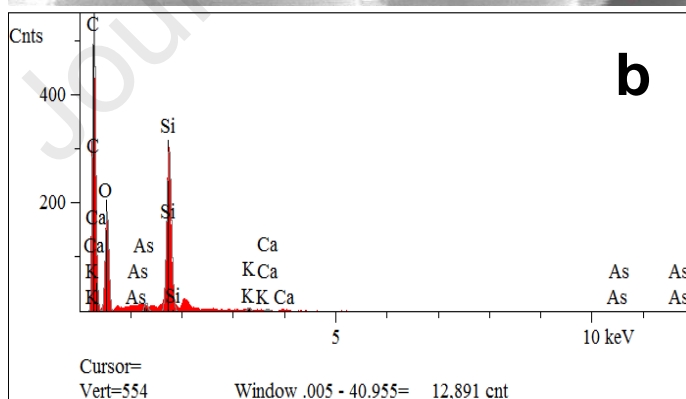
827

828

829

830

831

832

833
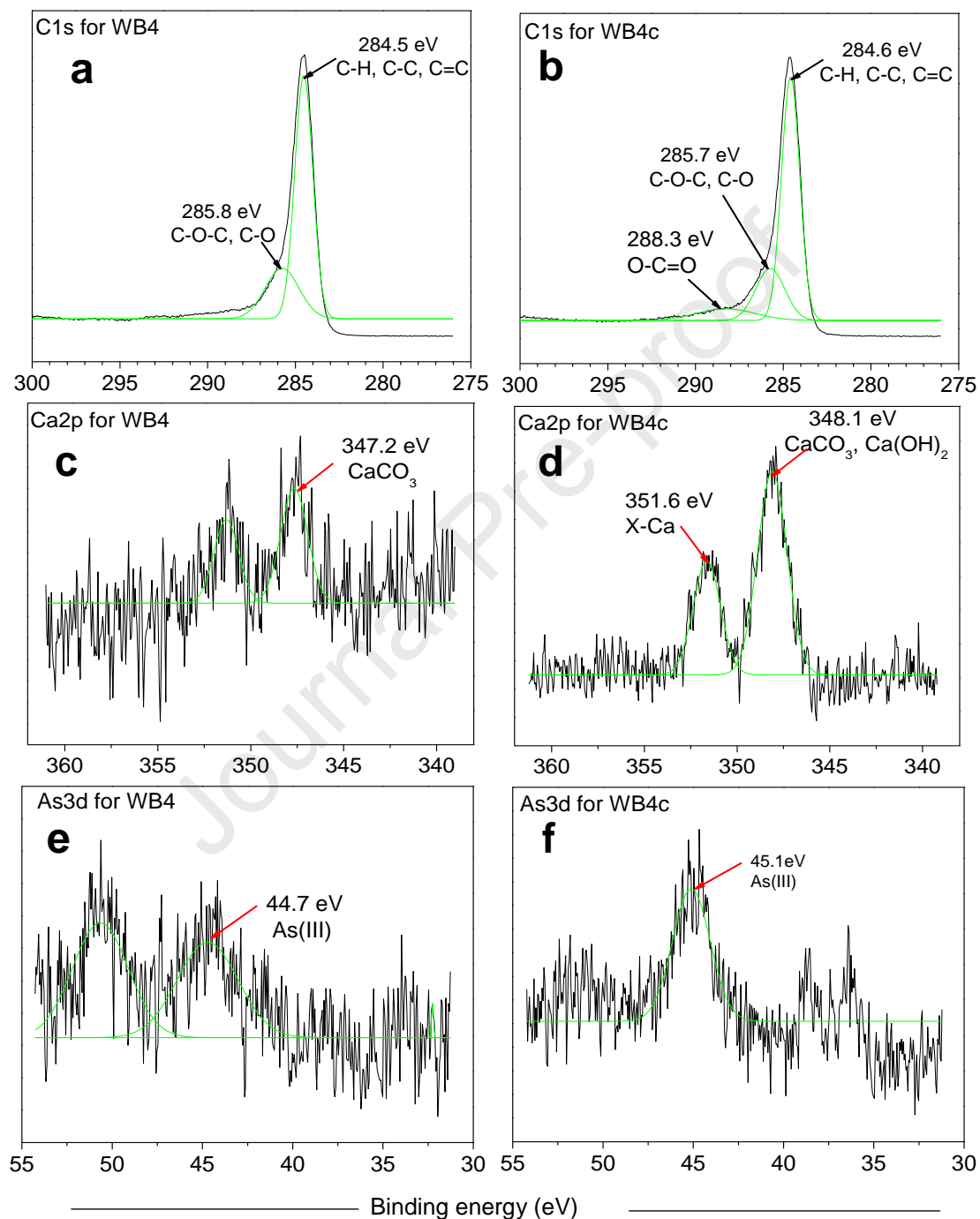
834

835

836

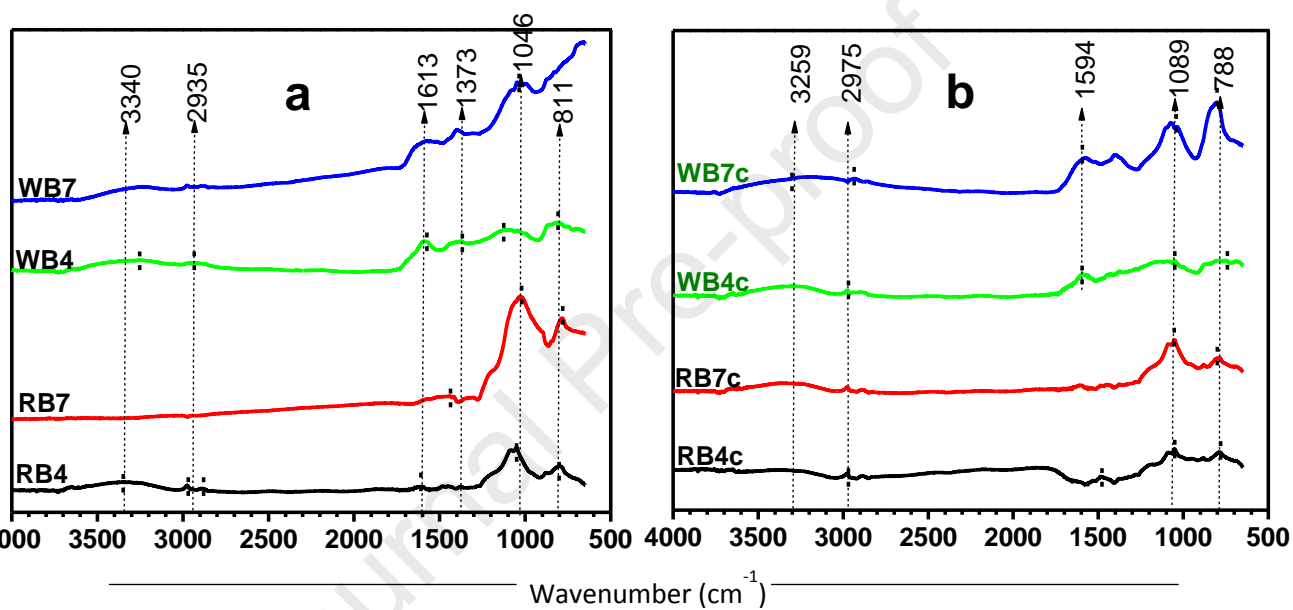837

838

839

840

841

842

843

844

845

846

847

848

849

850

851

Figure 7

852

853

854
a C1s for WB4

284.5 eV
C-H, C-C, C=C

285.8 eV
C-O-C, C-O

855

856

857

858

859

860
300 295 290 285 280 275

b C1s for WB4c

284.6 eV
C-H, C-C, C=C

285.7 eV
C-O-C, C-O

288.3 eV
O-C=O

300 295 290 285 280 275

861
c Ca2p for WB4

347.2 eV
CaCO$_3$

862

863

864

865

866

867
360 355 350 345 340

d Ca2p for WB4c

348.1 eV
CaCO$_3$, Ca(OH)$_2$

351.6 eV
X-Ca

360 355 350 345 340

868
e As3d for WB4

44.7 eV
As(III)

869

870

871

872

873

874

875
55 50 45 40 35 30

f As3d for WB4c

45.1eV
As(III)

55 50 45 40 35 30

Binding energy (eV)

876

877

878

879

880

881

882

883

884

885

886

887 **Figure 8**

888

897

898 Wavenumber (cm^{-1})

899

900

901

902

903

904

905

906

907

908

909

910

Highlights

- Biochar was used to improve the precipitation of arsenic with calcium compounds.

- Added biochar doubled the removal of arsenic by 58.1% compared to 25.4% without biochar.

- Precipitates formed included $Ca(AsO_2)_2$, $CaAsO_2OH \cdot \frac{1}{2}H_2O$, $Ca_5(AsO_4)_3OH$, deposited in biochar pores.

- The pH of solution and biochar type significantly affected the precipitation process.

- Arsenic desorption was lowest on wood biochar (< 0.3 %) compared to rice husk biochar (3.2 %).

Declaration of interests

☒ The authors declare that they have no known competing financial interests or personal relationships that could have appeared to influence the work reported in this paper.

☐The authors declare the following financial interests/personal relationships which may be considered as potential competing interests: